A Novel Bi_2O_3 Modified C-doped Hollow TiO_2 Sphere Based on Glucose-derived Carbon Sphere with Enhanced Visible Light Photocatalytic Activity

Fengjin Chai[1] · Fuliang Meng[2] · Shuai Liu[1] · Yu Zhang[1] · Tao Yang[1] · Yufei Jia[1] · Songjun Li[1,3] · Xinhua Yuan[1]

Abstract

The hydrothermal method was used to synthesize carbon sphere, and the hard template synthesis method was used to prepared C-doped hollow TiO_2 sphere (CHTS). Bismuth nitrate was used as bismuth source to modify CHTS. The composite material was oxidized in air atmosphere at 450℃ to obtain Bi_2O_3 modified C-doped TiO_2 hollow spheres(BCHTS). The morphology, elemental composition and photocatalytic degradation efficiency of tetracyclines (TC) by BCHTS hollow spheres were characterized by various measurements. Additionally, the possible transformation pathways and degradation mechanism of tetracycline were revealed via LC–MS and trapping experiments. The experimental results show that the Bi nanoparticles are uniformly dispersed in the CHTS. The photocatalyst exhibits enhanced degradation rate of TC (98.4% under visible-light within 180 min and 99.4% under natural light within 50 min) for its structure and narrow bandgap (2.87 eV). After five degradation cycles, the photocatalyst still remains high removal rate of 96.4% for TC. The results indicate that the photocatalyst may be promising for degrading antibiotic residuals remains. According to the trapping experiment, OH and h^+ have a certain role on the photodegradation process, while $·O^{2-}$ is the main active species for degrading TC.

Keywords Inorganic organic composite · Bismuth oxide · Bi_2O_3 modified C-doped TiO_2 · Hollow sphere · Photocatalytic degradation · Tetracyclines

1 Introduction

In recent years, antibiotics have been widely used not only in human medical care, but also in aquaculture and animal husbandry for medical and non-medical enhanced crop production. However, the overuse of antibiotics causes their residues to be widely dispersed in the environment, posing a serious threat to human and ecosystem health [1, 2]. Therefore, the development of effective methods to degrade or remove antibiotic residues from the aquatic environment is critical.

At present, these current methods can be loosely classified into three types: physical removal (adsorption, sedimentation, flocculation and filtration) [3, 4], biological treatment [5, 6] and chemical degradation (ozonation, chlorination, and Fenton's oxidation) [7–9]. Alternatively, photocatalysis is gaining increasing global interest and is widely implemented in new energy extraction and environmental control strategies with substantial progress made in recent years [10, 11]. Cai [12] found that Cr^{3+} doping $SrTiO_3$ cubic nanoparticles could only degrade 70% of tetracycline (TC) under visible light. Zhang [13] prepared Ce^{3+} doped Bi_2O_3 hollow needle-shape with removal rate of 89% for TC. Additionally, Wang [14] realized the degradation 94% of TC over Bi^{3+} doped ultrathin g-C_3N_4 nanosheets under visible light. However, it is still a big challenge to further improve the degradation efficiency of photocatalyst for antibiotics under visible light.

For a long time, TiO_2 has attracted much attention as a photocatalytic material due to its advantages of good

✉ Songjun Li
Lsjchem@ujs.edu.cn

✉ Xinhua Yuan
yuanxh@ujs.edu.cn

[1] School of Materials Science and Engineering, Jiangsu University, ZhenjiangJiangsu 212013, China

[2] Hangmo New Materials Group Co., Ltd, Huzhou 313310, Zhejiang, China

[3] Research School of Polymeric Materials, Jiangsu University, Zhenjiang 212013, Jiangsu, China

photochemical stability, non-toxicity, photocatalytic activity and low cost [15]. However, the broadband gap results in that TiO_2 can only absorb ultraviolet light (4% of the solar spectrum) [16, 17].

In order to further improve the photocatalytic activity of TiO_2, researchers have tried various methods. From the perspective of structure, hollow spherical nanostructures can make light reflect and scatter multiple times within the shell, thus extending the path of light to enhance the absorption capability [18–22]. Appropriate doping of metallic or nonmetallic elements can produce intermediate energy levels within the band gap, providing a springboard for electron conversion, which allows low-energy photons to be adsorbed to longer wavelengths, thus extending the range of light absorption. Carbon doping exhibits considerable potential advantages over non-metal doping. Firstly, carbon presents metallic conductivity [23]. Secondly, carbon has a large electron-storage capacity and can accept the photon-excited electrons to enhance the separation of photo-generated carries [24]. More particularly, carbon element is always indicated permeating to the lattice of TiO_2 and forms O–Ti–C bond in the process of doping, which produces a hybrid orbital above the valence band of TiO_2 and extends the visible-light absorption [25]. On the other hand, α-Bi_2O_3 has superior visible light absorption capacity for its band gap of 2.85 eV and dye sensitization effect [26, 27]. However, pure Bi_2O_3 photocatalyst has some problems such as poor structural stability and the fast recombination of photogenerated charge carriers, which limits the application of Bi_2O_3 in photocatalysis [28, 29]. To address the problem, C-doped hollow TiO_2 sphere with stable structure was used as primary catalyst and Bi_2O_3 nanoparticles was used as cocatalyst, respectively.

Though the C-doped TiO_2 or Bi_2O_3/TiO_2 composites were prepared and studied by some research workers [30–32], there are no report about Bi_2O_3 modified C-doped TiO_2. In this paper, the carbon spheres were prepared by glucose hydrothermal method as substrate, and C-doped TiO_2 hollow spheres were prepared by template sacrifice method. The prepared C-doped TiO_2 hollow spheres were used to adsorb Bi^{3+}, and Bi^{3+} was oxidized to Bi_2O_3 by calcination in air environment at 450℃. Finally, C-doped TiO_2 hollow spheres modified by Bi_2O_3 were obtained. The composite has excellent photocatalytic activity for its outstanding redox capability, visible-light absorption ability.

2 Experimental Section

2.1 Materials

Glucose anhydrous ($C_6H_{12}O_6$, AR), hexadecetyltrimethyl ammonium bromide (CTAB, AR), tetrabutyl titanate (TBOT, CP), bismuth nitrate [$Bi(NO_3)_3$]•5H_2O, AR], bismuth oxide(Bi_2O_3, AR), ethanol (C_2H_5OH, AR), and tetracyclines (TC, CP) were purchased from Sinopharm Corporation Ltd. (Shanghai, China). 0.04 M dilute nitric acid was prepared with nitric acid (HNO_3 at 68%, CP) purchased from Sinopharm Corporation Ltd. Deionized water was employed in all experiments. All chemicals were used without further purification.

2.2 Experimental

2.2.1 Preparation of Carbon Sphere Templates

In a typical procedure [33–35], 14.4 g of glucose was firstly dissolved in deionized water (80 mL). Then the solution was transferred into a 100 mL Teflon-lined stainless steel autoclave. Finally, hydrothermal treatments were carried out at 240 ℃ for 4 h and then cooled down to room temperature naturally. The obtained products were filtered and washed with alcohol and deionized water for several times, then dried at 60 ℃ for 12 h.

2.2.2 Preparation of C-doped TiO_2 Hollow Spheres

The prepared carbon spheres (0.4 g) were firstly dispersed in ethanol (30 mL). The cetyltrimethyl ammonium bromide (CTAB, 0.2 g) was dissolved in 70 mL ethanol and 0.4 mL deionized water mixture solution, and then the prepared carbon spheres solution was added into the CTAB solution. After stirring 2 h, tetrabutyl titanate (TBOT, 2 mL) in ethanol (20 mL) was injected by dropping. Subsequently, the solution was stirred for 24 h at room temperature. The final products were centrifuged and washed with ethanol and dried at 60 ℃ for 10 h. In addition, the product was calcined at 450 ℃ for 2 h to remove the carbon sphere. The sample was denoted as CHTS. For comparison, the TiO_2 nanoparticles (TNP) were prepared without carbon sphere addition by the same process.

2.2.3 Preparation of Bi_2O_3 Modified C-doped TiO_2 Hollow Spheres

The prepared CHTS (50 mg) was dispersed in 50 mL ethanol, and 10 mL HNO_3 (0.04 M) mixed with $Bi(NO_3)_3$·5H_2O (20 mg) was added into the solution and stirred for 2 h. Subsequently, the solution was stirred at 60 ℃ until it was evaporated. The products were calcined at 450 ℃ for 2 h. The sample was denoted as BCHTS. The whole prepare process is shown in Fig. 1.
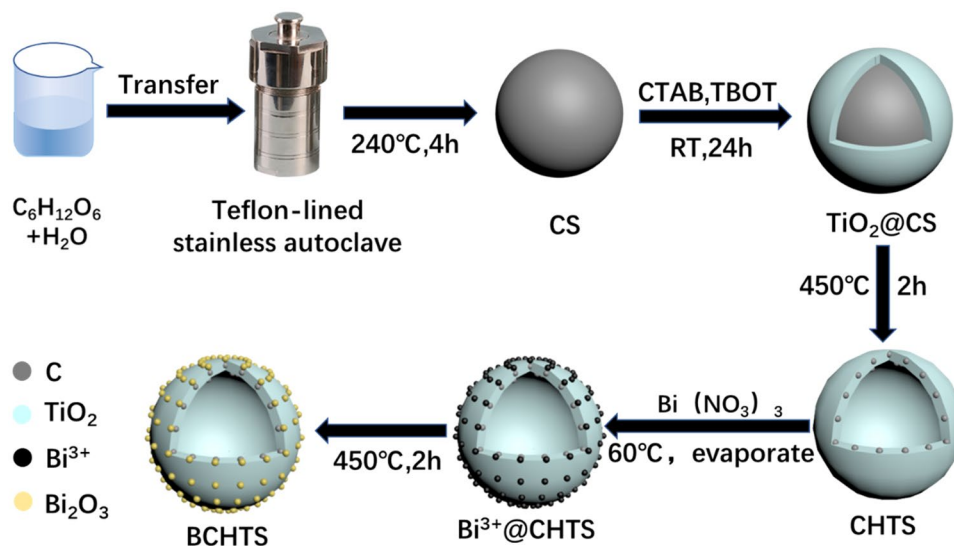
2.3 Characterization

The crystal structure and composition were carried out on a D8 ADVANCE powder X-ray diffractometer (XRD), and a scanning rate of 5°/min was used to record the patterns in the 2 theta angle ranging from 5° to 90°. JEM-2100(HR) transmission electron microscope (TEM) and FEI NovaNano450 scanning electron microscope (SEM) were used to characterize the morphology of the samples. The elemental composition was tested on a Thermo Scientific K-Alpha X-ray photoelectron spectrometer (XPS). Identification of the intermediates in the photodegradation of TC was analyzed by a liquid chromatography–mass spectrometry (LC–MS, Thermo LXQ LC/MS), and the mass range is from m/z 50 to 600.

2.4 Photocatalytic Activity Measurements

The photocatalytic activity of the catalysts was evaluated by the degradation of tetracyclines (TC) under visible light irradiation. A 300 W Xenon lamp was used as the simulated solar light. The 420 nm cut off filter was used to get the visible light source. In each experiment, 10 mg of the as-prepared photocatalyst was added into 50 mL tetracyclines solution (10 mg/L). Before irradiation, the suspensions were placed in dark and stirred for 30 min to ensure the establishment of adsorption–desorption equilibrium between the catalyst and tetracyclines. Subsequently, at every interval, about 3 mL suspension was sampled and centrifuged to remove the photocatalyst particles. The concentration of filtrates was analyzed by measuring the maximum absorbance at 357 nm for tetracyclines using a UV-2600 UV–vis spectrophotometer.

The degradation rate of the catalyst to the dye can be expressed as:

$$\text{Degradation rate} = (C_0 - C)/C_0 \times 100\% \tag{1}$$

In the formula (1), C_0 represents the initial concentration (mg/L) of the TC solution, and C represents the current concentration (mg/L) of the TC solution measured at the time of sampling.

3 Results and Discussion

3.1 SEM and TEM Analyses

SEM images of CS, CHTS and BCHTS are shown in Fig. 2. The prepared carbon sphere template (Fig. 2a) is smooth and regular spherical shape, and the carbon spheres are connected with each other by some degree of adhesion, while the diameter of the sphere is about 500–720 nm. After coating the surface of the carbon spheres with a layer of TiO$_2$ and removing the template of the carbon spheres (Fig. 2b), the surface of the sample become rough, and the diameter is increased to about 550–780 nm, which indicates that TiO$_2$ is successfully coated on the surface of the carbon spheres with a thickness of about 50 nm. At the same time, some broken spheres can be seen in Fig. 2b, which indicates that the template of the carbon spheres has been removed, and the catalyst prepared is a hollow spherical structure. After loading Bi$_2$O$_3$ (Fig. 2c), the diameter and morphology of the catalyst do not change greatly, while the surface becomes more rough, and there are many raised small particles, indicating that Bi$_2$O$_3$ is loaded on the C-doped TiO$_2$ hollow sphere in the form of nanoparticles. In addition, there are some fine nanoparticles, which may be caused by the collapse of some structures due to calcination of the catalyst. Figure 2d shows the TEM image of BCHTS. It can be further seen that the catalyst is a piece of interconnected hollow spherical
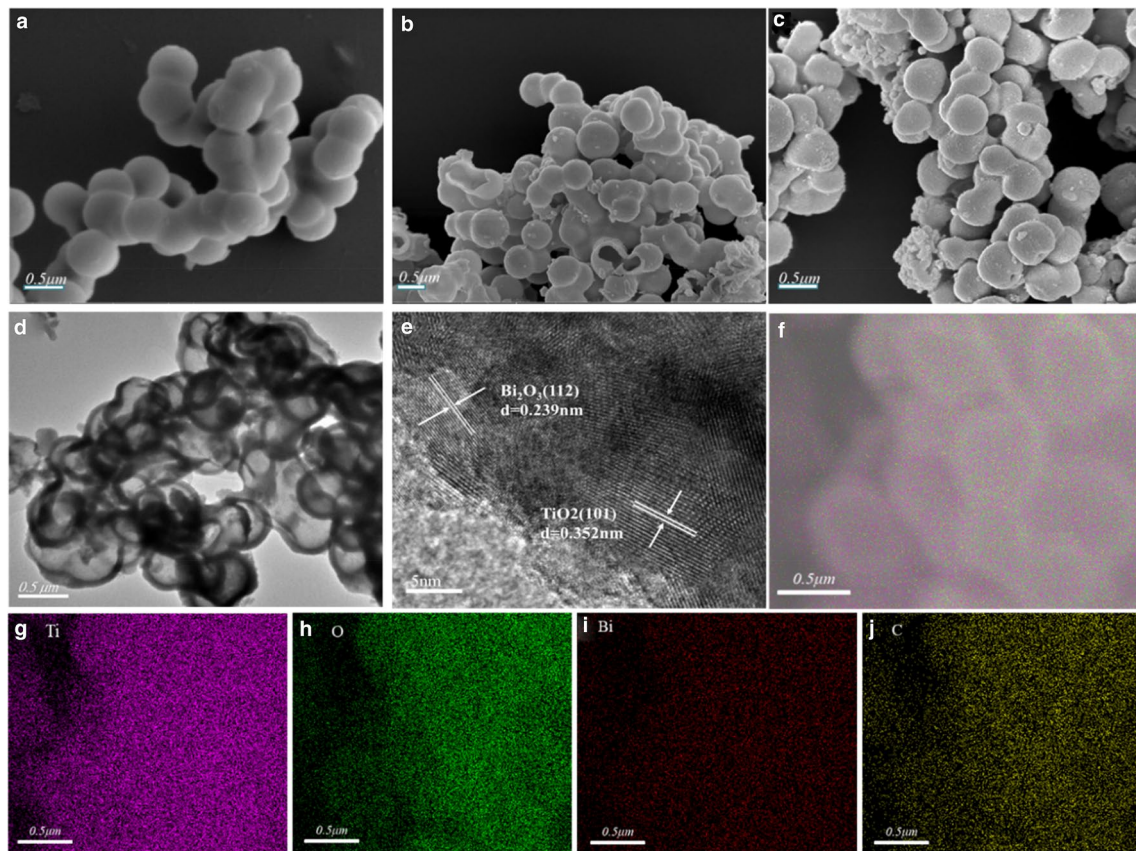
Fig. 2 SEM of CS (**a**), CHTS (**b**), and BCHTS (**c**), TEM (**d**), HRTEM(**e**) and mapping (**f-j**) of BCHTS

structure. The HRTEM (Fig. 2e) shows that BCHTS consists of α-Bi_2O_3 with lattice spacing of 0.239 nm (112)[36] and anatase TiO_2 with lattice spacing of 0.352 nm (101)[37], which reveals the successive coupling of TiO_2 and Bi_2O_3. Meanwhile, SEM mapping of BCHTS in Fig. 2f-j indicates that BCHTS contains Ti, O, Bi and C elements. Bi signal is evenly distributed in the sample (Fig. 2i), and some C elements are doped in the sample during the removal of the hard template (Fig. 2j).

3.2 XPS and XRD Spectra

The XPS survey spectrum of BCHTS confirms the existence of Ti, O and Bi (Fig. 3a). As shown in Fig. 3b, Ti 2p spectrum of BCHTS is observed, and the binding energy of Ti 2p are 458.3 eV ($2p_{3/2}$) and 464.0 eV ($2p_{1/3}$)[38]. Besides, the XPS spectra of O 1 s can be fitted into two peaks at 529.5 eV and 531.0 eV (Fig. 3c). The peak at 529.5 eV is attributed to the lattice oxygen, while the latter one is assigned to the defect sites with a low oxygen coordination. This may suggest the generation of oxygen vacancies [39, 40]. For Fig. 3d, we find four broad peaks in the Bi 4f spectrum. Two prominent peaks at 158.9 eV

and 164.2 eV are ascribed to characteristic arbital splitting of Bi $4f_{7/2}$ and Bi $4f_{5/2}$, respectively, while two peaks at 157.2 eV and 162.7 eV are attributed to metallic Bi^0 [41]. This may suggest that some of Bi^{3+} were reduced at the process of preparation. There are three peaks in the C 1 s spectrum (Fig. 3e). The peaks at 285.8 eV and 288.2 eV are characteristic peaks of the oxygen bound species C–O and C-Ti–O, respectively. These indicate that carbon elements are always indicated permeating to the lattice of TiO_2 and form O–Ti–C bond in the process of doping [42].

The XRD patterns of CHTS and BCHTS are described in Fig. 3f. The peaks of CHTS at values of 25.3, 38.0, 48.0, 53.7, 55.0 and 62.5°are respectively attributed to (101), (004), (200), (105), (211) and (204) crystal planes of typical TiO_2[43]. All peaks are indexed to the anatase of TiO_2 (JCPDS: 21–1272). Meanwhile, some peaks of BCHTS well correspond to the standard of anatase, and the other characteristic diffraction peaks can also be indexed to the $Bi_2O_{2.33}$ (JCPDS: 27–0051)[44]. This suggests that part of Bi^0 are contained in the sample apart from Bi_2O_3. All results are consistent with XPS spectrum, which further proves that Bi is uniformly dispersed in the sample.

Fig. 3 XPS spectra of BCHTS (**a**), Ti 2p (**b**), O 1 s (**c**), Bi 4f (**d**), and C 1 s (**e**). XRD patterns (**f**)
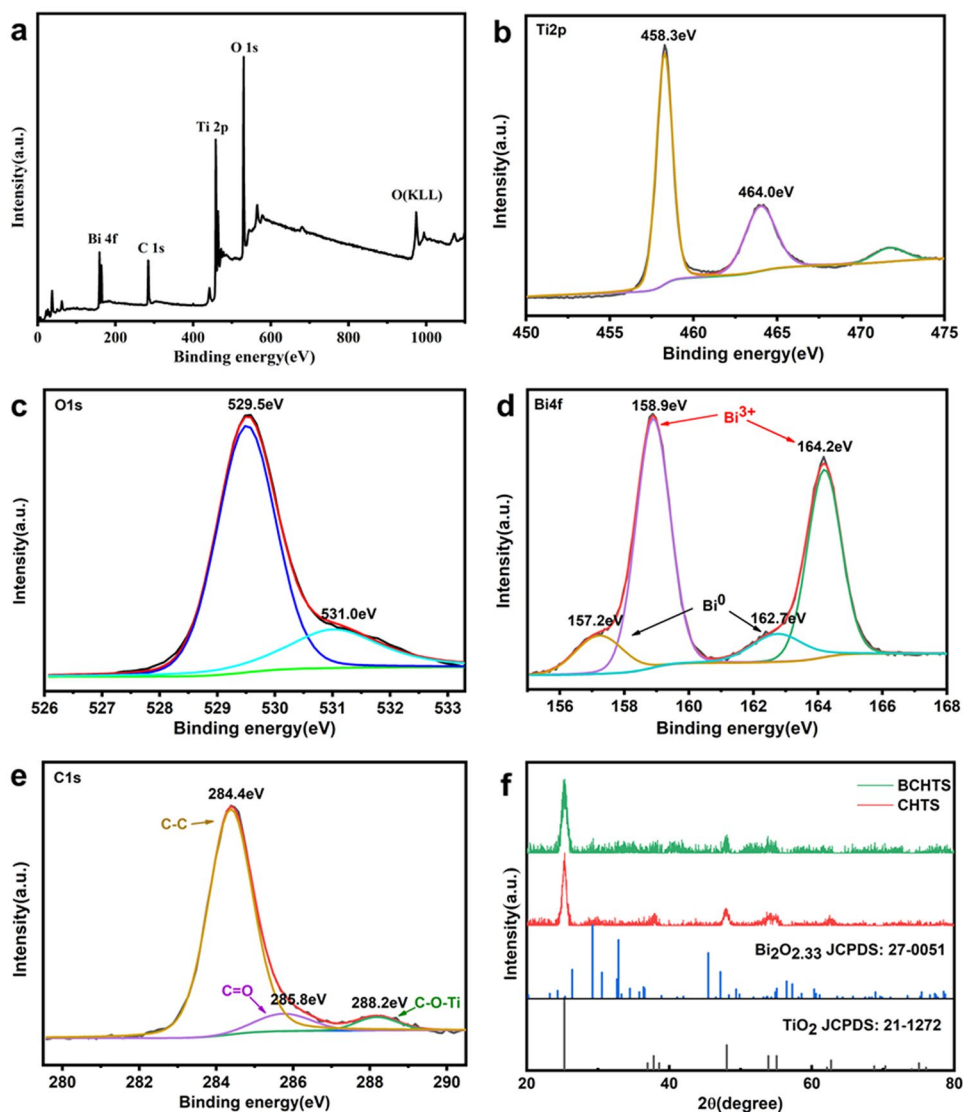

3.3 UV–Vis Analysis

The light-harvesting capability and the corresponding forbidden bandwidth obtained by Kubelka–Munk model of CHTS and BCHTS were analyzed via UV–Vis absorption spectra. As shown in Fig. 4a, besides strong UV light absorption, BCHTS exhibits a weak visible light absorption than CHTS. According to the Kubelka–Munk model (Fig. 4b), the bandgap of CHTS (3.12 eV) is similar to anatase (3.2 eV). Meanwhile, BCHTS shortens its bandgap from 3.12 to 2.87 eV after modified by Bi_2O_3. This result show that BCHTS is more prone to be excited under

Fig. 4 UV–vis absorption (**a**) and bandgap (**b**) of CHTS and BCHTS
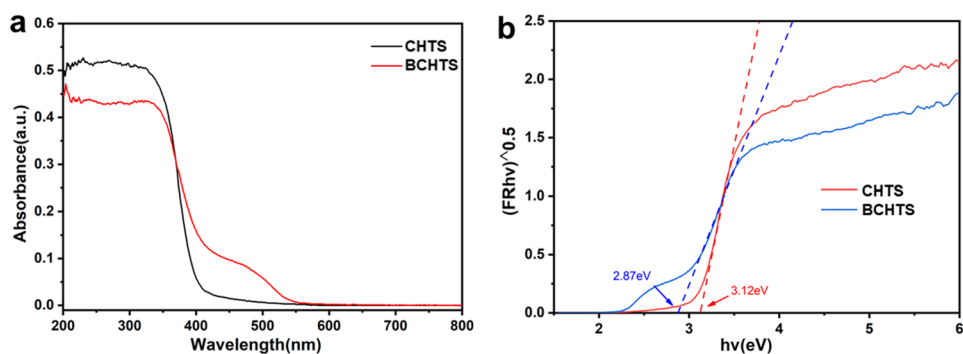
visible light due to its more narrow forbidden bandwidth [45].

3.4 Photocatalytic Performance

The photocatalytic performance of BCHTS was investigated by degrading TC which was widely used as contaminants under visible-light. As shown in Fig. 5a, the obvious absorption peak of TC can be observed at value of 357 nm. After stirred for 30 min in the darkness, the absorption peak of TC just becomes lower without any changes, and the characteristic peak (357 nm) is gradually decreased and disappeared when TC is illuminated under visible-light. This suggests that the prepared BCHTS can efficiently degrade TC under visible-light. The photocatalytic performance of BCHTS under different lights is shown in Fig. 5c. The degradation of TC is almost unchanged after stirring for 30 min in the darkness, which indicates that the absorption equilibrium is achieved after only 30 min stirring. The TC is degraded completely after 50 min under natural light. Meanwhile, to better evaluate the photocatalytic activity, Bi_2O_3, CHTS, and TNP were used as reference samples (Fig. 5d). Under visible-light irradiation, the degradation rates of TC are only about 32.2% and 79.7% within 180 min for Bi_2O_3 and TNP, respectively. Compared to them, the degradation of TC for CHTS and BCHTS can reach 89.9% and 98.4% within 180 min under visible-light, which well manifest that both the hollow sphere structure and the modification of Bi_2O_3 have great effects on the improvement of the photocatalytic performance of TiO_2. Specially, the removal of TC almost come up to 100% with the help of BCHTS under visible light, which is higher than the photocatalysts in previous researches [12–14, 46].

3.5 Possible Transformation Pathways of TC

In order to identify the potential structure of photodegradation products, the MS determination was performed. The MS spectra of TC degradation solution after 100 and 180 min irradiation can be seen in Fig. 6, which reveals the occurrence of several peaks and attributes to the photodegradation products with m/z values of 475, 461, 438, 415, 393, 349, 361, 305, 242, 210 and 175. Based on the photodegradation intermediate products, the transformation pathway is proposed as shown in Fig. 7, which can be outlined by three routes.

During the whole transformation process, the intermediates are mainly generated by two routes with the loss of functional groups and the open-ring reactions. For pathwayI, the TC 1 (m/z = 445) are attacked by reactive oxygen species to the double bond to obtain the oxidative compound TC 2 (m/z = 461). Then, TC 3 (m/z = 349) was formed during the deamination reaction, the breaking and oxidation of the ester bond, the carbon–carbon double bond and the ring. As the photodegradation is progressed, the ring opening reactions and the oxidative decomposition are further occurred to form TC 4 (m/z = 305) and TC 5 (m/z = 261) [47]. For pathway II, TC 6 (m/z = 475) is formed from the addition reaction, the rearrangement with the ·OH radicals and the oxidation of N-methyl to N-aldehyde group. Then

Fig. 5 UV–vis spectra of TC at different time of photodegradation (**a**). Photocatalytic performances of BCHTS under different light (**c**) and different samples (**d**)
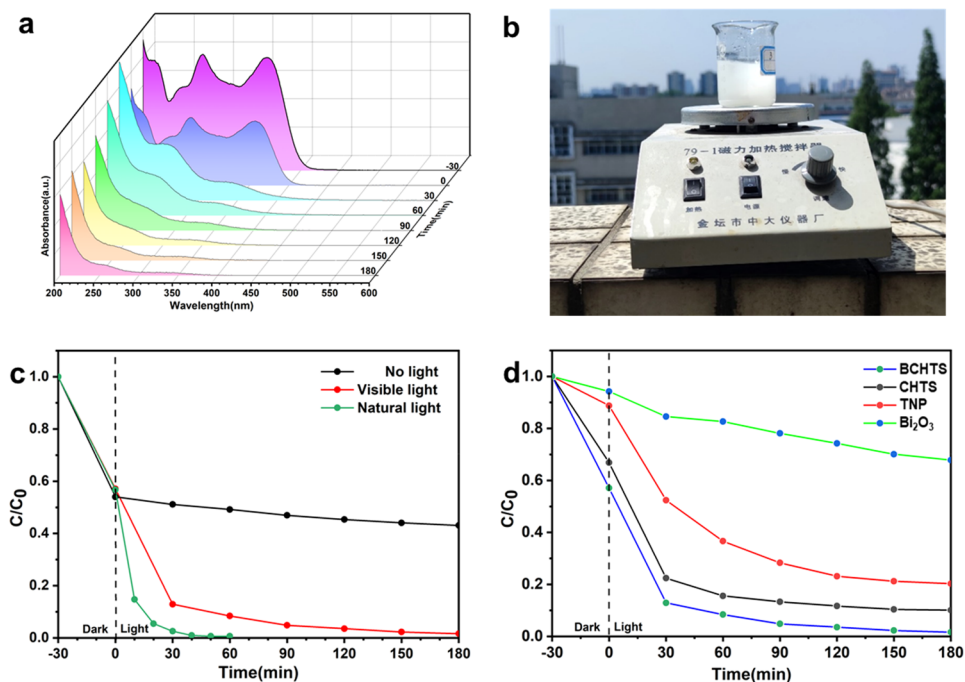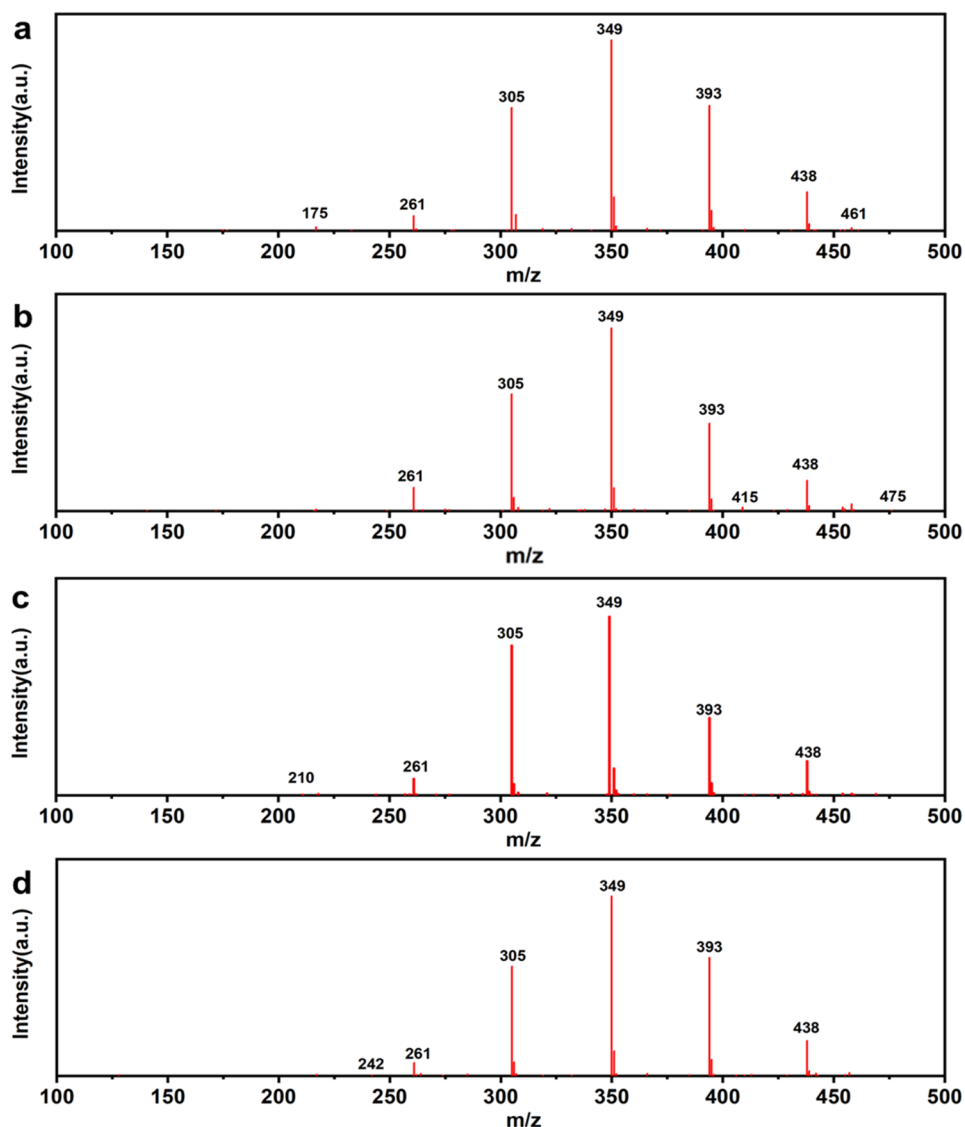
Fig. 6 The corresponding MS spectrum of the intermediate products

TC 6 might be transferred to TC 7 (m/z = 438) through dislodging N–C bond and hydroxyl-substitution reaction by the attack of ·OH radicals. TC 7 is transferred into TC 8 (m/z = 210) via the loss of methyl and hydroxyl group and the rupture of C–C single bond leading to the breakage of ring [48]. For pathway III, TC 1 is first transformed into TC 9 (m/z = 415) which is also proved by other researches [49, 50]. The TC 10 (m/z = 393) is generated from TC 9 by the dealkylation, deamination and dehydration process. Then TC 11 (m/z = 242) and TC 12 (m/z = 175) are formed via ring-opening process [51].

3.6 Photodegradation cycle of TC

The reusability of photocatalysts are crucial for the potential application in wastewater disposal. Therefore, the cycle experiment was conducted over BCHTS toward the

degradation of TC. After each test, the photocatalyst was filtrated, washed and finally dried at 60 °C for 12 h. Figure 8a and Fig. 8b show that after five photodegradation cycles of TC, the degradation rate of TC still remains 96.4%, which indicates that the degradation activity of BCHTS is almost excellent even after five degradation processes. This suggests that the prepared BCHTS photocatalyst has superior reusability. Notably, XRD test (Fig. 8c) shows that the crystal structure of BCHTS remains unchanged after five cycles, which indicates that BCHTS has excellent stability and sustainability of structure. This is the reason for the superior cycling performance of BCHTS.

3.7 Trapping Experiment

To learn more photodegradation mechanism of TC, the role of active species was investigated via trapping experiment.

Nitrogen, isopropyl alcohol (IPA) and triethanolamine (TEA) were employed to quench·O^{2-}, ·OH and h^+, respectively. When N_2 is pumped into the reaction system, the generation of ·O^{2-} is limited by the absence of O_2. Different from the restraints of ·O^{2-} by N_2, ·OH and holes are restrained by quench technique. The principle of this method is that active species can be quenched by certain substances,

and cannot play their original role. The specific experimental method is to add a specific quenching agent (sometimes called scavenger) in the photocatalytic degradation process. When the active species were restrained, we can observe whether the removal of pollutants is lower. If the removal is lower, it indicates that the contribution of the active species in the degradation process is higher. Figure 9a and Fig. 9b
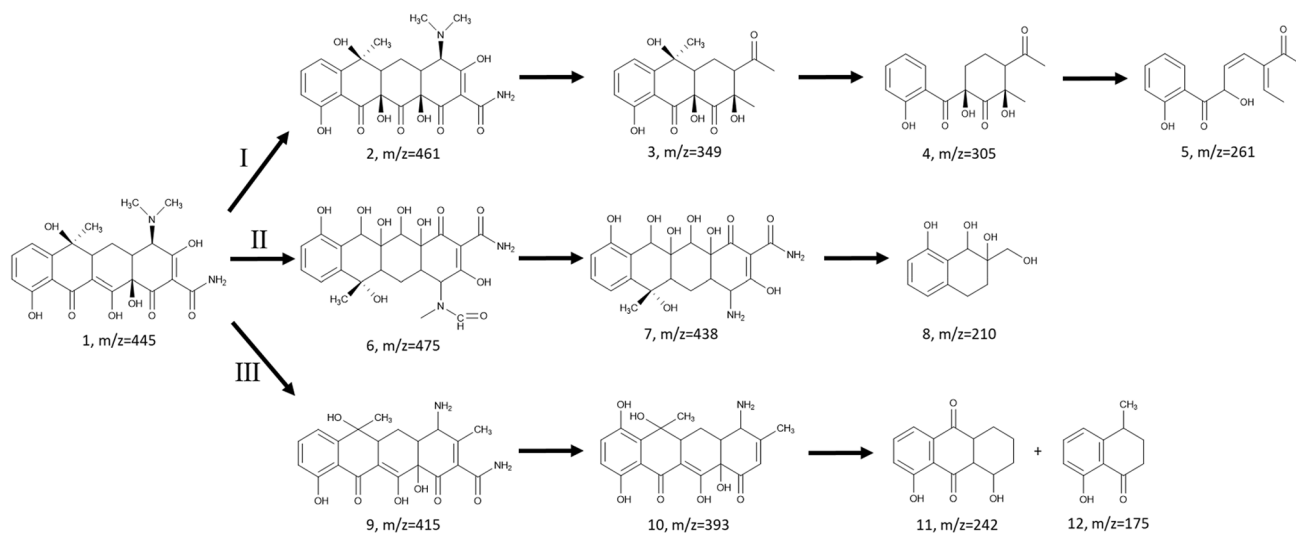

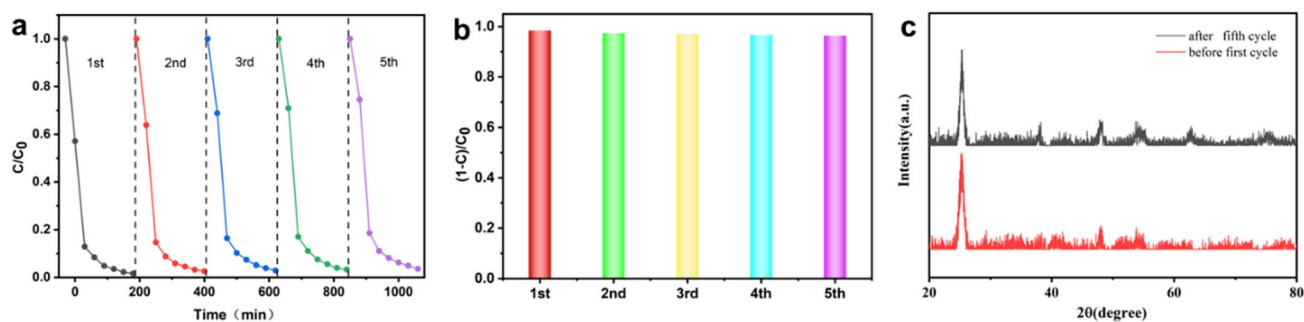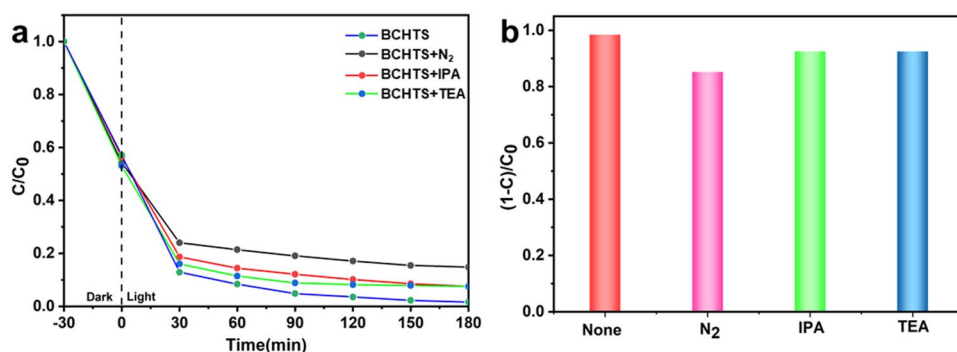Fig. 7 Possible transformation pathways of TC degradation

Fig. 8 Photodegradation cycle of TC (**a**, **b**) and XRD of BCHTS before first cycle and after fifth cycle (**c**)

Fig. 9 Photodegradation of TC with different quenchers in the trapping experiment

show that the addition of IPA and TEA makes the degradation of TC reduce to 92.4%, which reveals that ·OH radicals and h^+ play a certain role during the photodegradation process. While bubbling N_2 greatly suppresses the removal of TC to 85.2%, indicating that $·O^{2-}$ radicals are the main active species for degrading TC under visible light irradiation [52–54].

4 Conclusions

To obtain enhanced photocatalytic activity under visible-light, the carbon spheres were prepared by hydrothermal process with glucose, and Bi_2O_3 modified C-doped TiO_2 hollow spheres were prepared by sol–gel method based on carbon spheres with subsequent deposition–precipitation and calcination under air atmosphere. The prepared hollow structured photocatalysts with diameter about 500–720 nm and shell thickness of 50 nm show highly efficient visible light induced photocatalytic activities. The degradation rates of TC reach 98.4% under visible-light within 180 min and 99.4% under natural light within 50 min, respectively. Besides, the BCHTS exhibits good stability even after five cycles. After five cycles, it still remains high removal of TC with degradation rate of 96.4%. Additionally, the possible transformation pathways and degradation mechanism of tetracycline were revealed via LC–MS and trapping experiments in this paper. The prepared hollow structured photocatalyst may be a promising photocatalyst for degrading organic pollutants and environmental remediation.

Declarations

Conflict of interests The authors have not disclosed any Conflict of interests.

References

1. X.R. Yang, Z. Chen, W. Zhao, C.X. Liu, X.X. Qian, M. Zhang, G.Y. Wei, E. Khan, Y.H. Ng, Y.S. Ok, Recent advances in photodegradation of antibiotic residues in water. Chem. Eng. J. **405**, 126806 (2021)
2. S. Rodriguez-Mozaz, S. Chamorro, E. Marti, B. Huerta, M. Gros, A. Sànchez-Melsió, C.M. Borrego, D. Barceló, J.L. Balcázar, Occurrence of antibiotics and antibiotic resistance genes in hospital and urban wastewaters and their impact on the receiving river. Water Res. **69**, 234–242 (2015)
3. J. Luo, X. Li, C. Ge, K. Müller, H. Yu, P. Huang, J. Li, D.C.W. Tsang, N.S. Bolan, J. Rinklebe, H. Wang, Sorption of norfloxacin, sulfamerazine and oxytetracycline by KOH-modified biochar under single and ternary systems. Biores. Technol. **263**, 385–392 (2018)
4. S. Jia, Z. Yang, K. Ren, Z. Tian, C. Dong, R. Ma, G. Yu, W. Yang, Removal of antibiotics from water in the coexistence of suspended particles and natural organic matters using amino-acid-modified-chitosan flocculants: a combined experimental and theoretical study. J. Hazard. Mater. **317**, 593–601 (2016)
5. A. Benay, M. Molly, H. Felipe, B. Jens, B. Kyle, Characterization and biological removal of organic compounds from hydraulic fracturing produced water. Environ. Sci. Process. Impacts **21**(2), 279–290 (2018)
6. L. Xu, Z. Chu, H. Wang, L. Cai, Z. Tu, H. Liu, C. Zhu, H. Shi, D. Pan, J. Pan, X. Fei, Electrostatically assembled multilayered films of biopolymer enhanced nanocapsules for on-demand drug release. ACS Appl. Bio Mater. **2**, 3429–3438 (2019)
7. O.A. Alsager, M.N. Alnajrani, H.A. Abuelizz, I.A. Aldaghmani, Removal of antibiotics from water and waste milk by ozonation: kinetics, byproducts, and antimicrobial activity. Ecotoxicol. Environ. Saf. **158**, 114–122 (2018)
8. M.R. Ramli, N.M.N. Sulaiman, M.A. Mohd, M.F. Rabuni, Performance of chlorination process during nanofiltration of sulfonamide antibiotic. Water Sci. Technol. **72**, 1611–1620 (2015)
9. Q.J. Xie, Z.D. Chen, C.L. Teng, J. Dai, Methylene blue photocatalytic efficiency analysis under different forms of load titanium dioxide thin film. J. Jiangsu Univ. **39**(6), 704–707 (2018)
10. C. Zhao, Z. Chen, R. Shi, X. Yang, T. Zhang, Recent advances in conjugated polymers for visible-light-driven water splitting. Adv Mater **32**, 1907296 (2020)
11. J. Huang, X. Yang, S. Hussain, J. Tao, G.-W. Liu, G.-J. Qiao, Cooperative enhancement solar hydrogen generation of reformed g-C_3N_4/TiO_2 mesocrystals composites. J. Nanoelectron. Optoelectron. **15**, 46–53 (2020)
12. F. Cai, Y. Tang, F. Chen, Y. Yan, W. Shi, Enhanced visible-light-driven photocatalytic degradation of tetracycline by Cr^{3+} doping $SrTiO_3$ cubic nanoparticles. RSC Adv. **5**, 21290–21296 (2015)
13. W. Zhang, S. Gao, D. Chen, Preparation of Ce^{3+} doped Bi_2O_3 hollow needle-shape with enhanced visible-light photocatalytic activity. J. Rare Earths **37**, 726–731 (2019)
14. M. Wang, C. Jin, Z. Li, M. You, Y. Zhang, T. Zhu, The effects of bismuth (III) doping and ultrathin nanosheets construction on the photocatalytic performance of graphitic carbon nitride for antibiotic degradation. J Colloid Interface Sci. **533**, 513–525 (2019)
15. S. Wu, X. Li, Y. Tian, Y. Lin, Y.H. Hu, Excellent photocatalytic degradation of tetracycline over black anatase-TiO_2 under visible light. Chem. Eng. J. **406**, 126747 (2021)
16. M. Liu, X. Qiu, M. Miyauchi, K. Hashimoto, Energy-level matching of Fe (III) ions grafted at surface and doped in bulk for efficient visible-light photocatalysts. J. Am. Chem. Soc. **135**, 10064–10072 (2013)
17. H. Zhang, W. Wang, H. Zhao, L. Zhao, L.-Y. Gan, L.-H. Guo, Facet-dependent interfacial charge transfer in Fe (III)-grafted TiO_2 nanostructures activated by visible light. ACS Catal. **8**, 9399–9407 (2018)
18. J. Li, X. Liu, Z. Sun, L. Pan, Mesoporous yolk-shell structure Bi_2MoO_6 microspheres with enhanced visible light photocatalytic activity. Ceram. Int. **41**, 8592–8598 (2015)
19. X. Zou, H. Fan, Y. Tian, M. Zhang, X. Yan, Microwave-assisted hydrothermal synthesis of Cu/Cu_2O hollow spheres with enhanced photocatalytic and gas sensing activities at room temperature. Dalton Trans. **44**, 7811–7821 (2015)

20. G. Tang, S. Liu, H. Tang, D. Zhang, C. Li, X. Yang, Template-assisted hydrothermal synthesis and photocatalytic activity of novel TiO_2 hollow nanostructures. Ceram. Int. **39**, 4969–4974 (2013)

21. L. Xu, H. Wang, Z. Chu, L. Cai, H. Shi, C. Zhu, D. Pan, J. Pan, X. Fei, Y. Lei, Temperature-responsive multilayer films of micelle-based composites for controlled release of a third-generation EGFR inhibitor. ACS Appl. Polym. Mater. **2**, 741–750 (2020)

22. L. Xu, X. Zhang, Z. Chu, H. Wang, Y. Li, X. Shen, L. Cai, H. Shi, C. Zhu, J. Pan, Temperature-responsive multilayer films based on block copolymer-coated silica nanoparticles for long-term release of favipiravir. ACS Appl. Nano Mater. **4**, 14014–14025 (2021)

23. K. Woan, G. Pyrgiotakis, W. Sigmund, Photocatalytic carbon-nanotube–TiO_2 composites. Adv. Mater. **21**, 2233–2239 (2009)

24. G. Zhang, F. Teng, Y. Wang, P. Zhang, C. Gong, L. Chen, C. Zhao, E. Xie, Preparation of carbon–TiO_2 nanocomposites by a hydrothermal method and their enhanced photocatalytic activity. RSC Adv. **3**, 24644–24649 (2013)

25. C. Di Valentin, G. Pacchioni, A. Selloni, Theory of carbon doping of titanium dioxide. Chem. Mater. **17**, 6656–6665 (2005)

26. J.H. Li, J. Ren, Y.J. Hao, E.P. Zhou, Y. Wang, X.P. Wang, R. Su, Y. Liu, X.H. Qi, F.T. Li, Construction of β-Bi_2O_3/$Bi_2O_2CO_3$ heterojunction photocatalyst for deep understanding the importance of separation efficiency and valence band position. J. Hazard. Mater. **401**, 123262 (2021)

27. L. Leontie, M. Caraman, M. Delibaş, G.I. Rusu, Optical properties of bismuth trioxide thin films. Mater. Res. Bull. **36**(9), 1629–1637 (2001)

28. Y. Zhu, C. Jiao, L. Han, Y. Gao, S. Li, X. Yuan, A novel PHEMA-based bismuth oxide composite with high photocatalytic activity. J. Inorg. Organomet. Polym. Mater. **30**, 4739–4752 (2020)

29. L. Jiang, X. Yuan, G. Zeng, J. Liang, X. Chen, H. Yu, H. Wang, Z. Wu, J. Zhang, T. Xiong, In-situ synthesis of direct solid-state dual Z-scheme WO_3/g-C_3N_4/Bi_2O_3 photocatalyst for the degradation of refractory pollutant. Appl. Catal. B **227**, 376–385 (2018)

30. J. Payormhorm, R. Idem, Synthesis of C-doped TiO_2 by sol-microwave method for photocatalytic conversion of glycerol to value-added chemicals under visible light. Appl. Catal. A **590**, 117362 (2020)

31. F.C. Correia, M. Calheiros, J. Marques, J.M. Ribeiro, C.J. Tavares, Synthesis of Bi_2O_3/TiO_2 nanostructured films for photocatalytic applications. Ceram. Int. **44**, 22638–22644 (2018)

32. Z. Bian, S. Wang, Y. Cao, X. Qian, H. Li, Self-assembly of active Bi_2O_3/TiO_2 visible photocatalyst with ordered mesoporous structure and highly crystallized anatase. J. Phys. Chem. C **112**, 6258–6262 (2008)

33. G. Wen, B. Wang, C. Wang, J. Wang, Z. Tian, R. Schlogl, D.S. Su, Hydrothermal carbon enriched with oxygenated groups from biomass glucose as an efficient carbocatalyst. Angew. Chem. Int. Ed. Engl. **56**, 600–604 (2017)

34. X. Sun, Y. Li, Colloidal carbon spheres and their core/shell structures with noble-metal nanoparticles. Angew. Chem. **116**, 607–611 (2004)

35. K.U. Lee, M.J. Kim, K.J. Park, M. Kim, O.J. Kwon, J.J. Kim, Catalytic growth of a colloidal carbon sphere by hydrothermal reaction with iron oxide (Fe_3O_4) catalyst. Mater. Lett. **125**, 213–217 (2014)

36. K.B. Kusuma, M. Manju, C.R. Ravikumar, V.G. Dileepkumar, A.N. Kumar, M.S. Santosh, H.C.A. Murthy, K. Gurushantha, G. Sharma, Probe sonicated synthesis of bismuth oxide (Bi_2O_3): photocatalytic application and electrochemical sensing of ascorbic acid and lead. J. Nanomater. **2022**, 1–13 (2022)

37. M.A. Mohamed, M.F.M. Zain, L. Jeffery Minggu, M.B. Kassim, J. Jaafar, N.A. Saidina Amin, Y.H. Ng, Revealing the role of kapok fibre as bio-template for In-situ construction of C-doped g-C_3N_4@C, N co-doped TiO_2 core-shell heterojunction photocatalyst and its photocatalytic hydrogen production performance. Appl. Surface Sci. **476**, 205–220 (2019)

38. H. Yin, X. Wang, L. Wang, Q. Nie, Y. Zhang, W. Wu, Cu_2O/TiO_2 heterostructured hollow sphere with enhanced visible light photocatalytic activity. Mater. Res. Bull. **72**, 176–183 (2015)

39. S. Zhu, W. Liao, M. Zhang, S. Liang, Design of spatially separated Au and CoO dual cocatalysts on hollow TiO_2 for enhanced photocatalytic activity towards the reduction of CO_2 to CH_4. Chem. Eng. J. **361**, 461–469 (2019)

40. V. Jiménez, A. Fernández, J. Espinós, A. González-Elipe, The state of the oxygen at the surface of polycrystalline cobalt oxide. J. Electron Spectrosc. Relat. Phenom. **71**, 61–71 (1995)

41. Z. Wang, S. Yan, Y. Sun, T. Xiong, F. Dong, W. Zhang, Bi metal sphere/graphene oxide nanohybrids with enhanced direct plasmonic photocatalysis. Appl. Catal. B **214**, 148–157 (2017)

42. B. Li, Z. Zhao, F. Gao, X. Wang, J. Qiu, Mesoporous microspheres composed of carbon-coated TiO2 nanocrystals with exposed 0 0 1 facets for improved visible light photocatalytic activity. Appl. Catal. B **147**, 958–964 (2014)

43. W. Liu, D. Chen, S.H. Yoo, S.O. Cho, Hierarchical visible-light-response Ag/AgCl@TiO_2 plasmonic photocatalysts for organic dye degradation. Nanotechnology **24**, 405706 (2013)

44. Y. Peng, K.K. Wang, T. Liu, J. Xu, B.G. Xu, Synthesis of one-dimensional Bi_2O_3-$Bi_2O_{2.33}$ heterojunctions with high interface quality for enhanced visible light photocatalysis in degradation of high-concentration phenol and MO dyes. Appl. Catal. B **203**, 946–954 (2017)

45. M. Ge, C. Cao, S. Li, S. Zhang, S. Deng, J. Huang, Q. Li, K. Zhang, S.S. Al-Deyab, Y. Lai, Enhanced photocatalytic performances of n-TiO_2 nanotubes by uniform creation of p–n heterojunctions with p-Bi_2O_3 quantum dots. Nanoscale **7**, 11552–11560 (2015)

46. X. He, T. Kai, P. Ding, Heterojunction photocatalysts for degradation of the tetracycline antibiotic: a review. Environ. Chem. Lett. **19**, 4563–4601 (2021)

47. Z. Ye, J. Li, M. Zhou, H. Wang, Y. Ma, P. Huo, L. Yu, Y. Yan, Well-dispersed nebula-like ZnO/CeO_2@HNTs heterostructure for efficient photocatalytic degradation of tetracycline. Chem. Eng. J. **304**, 917–933 (2016)

48. M. Cao, P. Wang, Y. Ao, C. Wang, J. Hou, J. Qian, Visible light activated photocatalytic degradation of tetracycline by a magnetically separable composite photocatalyst: graphene oxide/magnetite/cerium-doped titania. J Colloid Interface Sci **467**, 129–139 (2016)

49. Y. Zhang, J. Zhou, X. Chen, L. Wang, W. Cai, Coupling of heterogeneous advanced oxidation processes and photocatalysis in efficient degradation of tetracycline hydrochloride by Fe-based MOFs: synergistic effect and degradation pathway. Chem. Eng. J. **369**, 745–757 (2019)

50. S. Wu, H. Hu, Y. Lin, J. Zhang, Y.H. Hu, Visible light photocatalytic degradation of tetracycline over TiO_2. Chem. Eng. J. **382**, 122842 (2020)

51. T. Zhang, Y. Liu, Y. Rao, X. Li, D. Yuan, S. Tang, Q. Zhao, Enhanced photocatalytic activity of TiO_2 with acetylene black and persulfate for degradation of tetracycline hydrochloride under visible light. Chem. Eng. J. **384**, 123350 (2020)

52. Y. Nosaka, A.Y. Nosaka, *Identification and roles of the active species generated on various photocatalysts* (Photocatalysis and Water Purification, Wiley, 2013), pp. 3–24

53. B. Luo, D. Xu, D. Li, G. Wu, M. Wu, W. Shi, M. Chen, Fabrication of Ag/Bi_3TaO_7 plasmonic photocatalyst with enhanced

photocatalytic activity for degradation tetracycline. ACS Appl. Mater. Interfaces **7**, 17061–17069 (2015)

54. J. Shen, R. Wang, Q. Liu, X. Yang, H. Tang, J. Yang, Accelerating photocatalytic hydrogen evolution and pollutant degradation by coupling organic co-catalysts with TiO_2. Chin. J. Catal. **40**, 380–389 (2019)

Publisher's Note Springer Nature remains neutral with regard to jurisdictional claims in published maps and institutional affiliations.